14th May 2011

Electrode Processes at Gas | Salt | Pd Nanoparticle | Glassy Carbon Electrode Contacts: Salt Effects on the Oxidation of Formic Acid Vapor and the Oxidation of Hydrogen

Fengjie Xia [a], Sara E.C. Dale [b], Richard A. Webster [b,c], Mu Pan *[a], Shichun Mu [a], Shik Chi Tsang [d], John M. Mitchels [e], and Frank Marken*[b]

[a] *State Key Laboratory of Advanced Technology for Materials Synthesis and Processing, Wuhan University of Technology, 430070, China*
[b] *Department of Chemistry, University of Bath, Claverton Down, Bath BA2 7AY, UK*
[c] *Doctoral Training Centre in Sustainable Chemical Technologies, University of Bath, Claverton Down, Bath BA2 7AY, UK*
[d] *Inorganic Chemistry Laboratory, University of Oxford, South Parks Road, Oxford, OX1 3QR, UK*
[e] *Microscopy and Analysis Suite, University of Bath, Claverton Down, Bath BA2 7AY, UK*

To be submitted to New Journal of Chemistry

Proofs to F. Marken

Email: F.Marken@bath.ac.uk

Abstract

The electrochemical oxidation of formic acid to CO_2 is facile at nano-palladium catalysts. In conventional electrochemical systems this process is conducted in aqueous phase and the resulting formation of poorly soluble CO_2 gas can limit the kinetics. Here, an alternative electrochemical system with the gas phase in closer contact to the palladium nanoparticle catalyst is investigated based on a glassy carbon electrode and a solid salt electrolyte. It is demonstrated that the reaction zone of salt (here $(NH_4)_2SO_4$ is most effective), palladium nanoparticle catalyst, and gas phase, is where the electrochemical oxidation process occurs. The effects of the type of salt, the partial pressure of formic acid, and the gas flow rate are investigated. Preliminary data for the oxidation of hydrogen gas at the salt | palladium | electrode contact are reported. A significant salt effect on the palladium catalysed reactions is observed and potential future applications of "salt cells" in sensing are discussed.

Keywords: palladium nanoparticles, hydrogen, formic acid vapour, carbon dioxide, fuel cell, salt – electrode contact, gas flow cell, voltammetry, sensor.

1. Introduction

Electrochemical measurements are commonly conducted in liquid electrolyte media with a reaction zone at the electrode | liquid interface. However, in many technically important applications of electrochemical processes more complex multi-phase systems with triple phase boundary reaction zones are required, for example, to allow a gas phase to interact simultaneously with electrode and electrolyte [1]. The study of these more complex multi-phase reaction zones is therefore of general interest. For the case of formic acid oxidation (as a more specific case), the low solubility of CO_2 in aqueous electrolyte media has been suggested to result in kinetic limitations when phase formation (e.g. gas evolution) occurs close to the catalyst [2]. One possible approach to resolving transport limitations and blocking effects in multi-phase electrode processes such as formic acid oxidation [3,4] is to introduce an electrode system with effective triple phase boundary reaction zone (see for example for formic acid oxidation [5] or for formic acid production [6]) including catalyst, electrolyte and gas phase.

Recently, it has been demonstrated that contact points of a solid salt (ammonium chloride) with a working electrode provide a suitable multi-phase environment for the study of electrochemical processes [7]. Under these conditions only a small fraction of the working electrode surface area is in contact to the salt electrolyte and electrochemically active. Therefore experiments are possible with lower currents and in two-electrode mode. The salt electrolyte provides surface conductivity sufficient for resistivity to be low, but the humidity level in the gas phase needs to be controlled in order to maintain a microscopic level of water for ion conduction across salt crystal surfaces and for processes to occur in salt | working electrode contact points [7]. In the previous report it was suggested that gas phase reactions at the salt | electrode contact could be of fundamental interest or

of use in sensor systems. Here, a palladium nanoparticle catalyst is immobilized at the working electrode surface and the catalyst | salt contact is investigated. The effects of the salt (high concentration effects and effects due to the type of salt) on the electrocatalytic reaction are studied for two cases: (i) the oxidation of formic acid vapor and (ii) the oxidation of hydrogen.

Formic acid is an interesting and potentially important liquid fuel system [8,9] and may be regarded as a direct liquid source of hydrogen [10,11] or energy [12]. Fuel cell prototypes have been proposed [13] and mostly nano-palladium [14] or palladium alloys [15] have been employed as a promising catalyst system. Here, a novel electrochemical cell configuration is investigated with nano-palladium in direct contact with solid salt electrolyte and the gas phase.

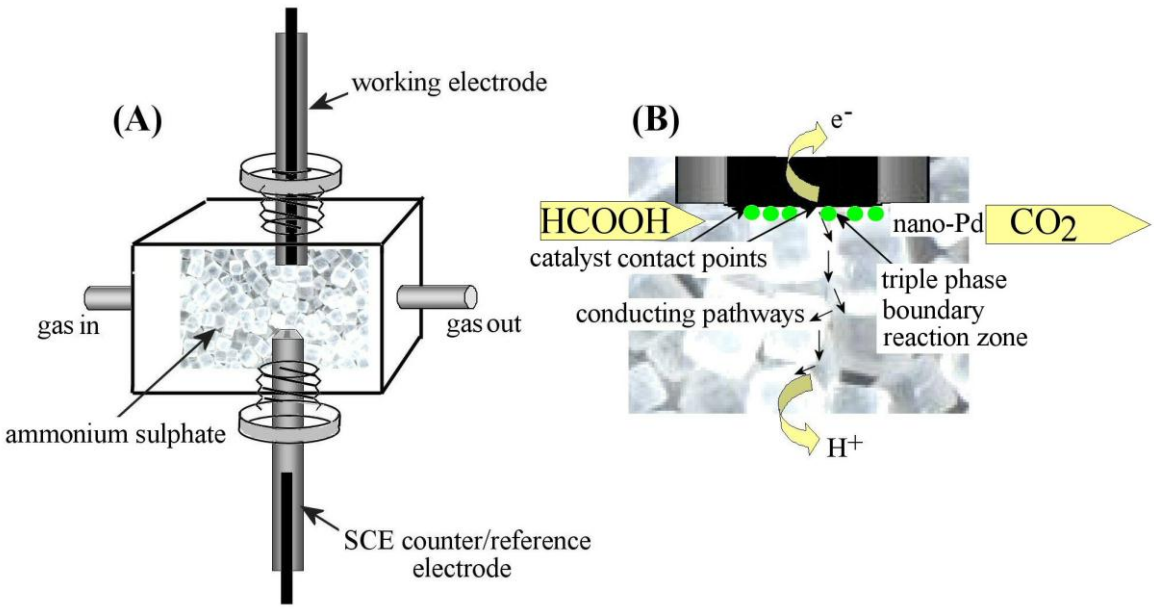

Figure 1. (A) Schematic drawing of the experimental electrochemical system [7] based on gas flow through a salt matrix separating the working and the counter/reference electrodes (B) Schematic drawing of the proposed processes during formic acid oxidation in the reaction zone at the catalyst-coated working electrode.

Figure 1 shows the electrochemical cell configuration [7] with a glassy carbon working electrode

(surface modified with nano-palladium) in contact to solid ammonium sulphate and an SCE counter/reference electrode. A nitrogen gas flow is maintained through this cell (pre-humidified in saturated $(NH_4)_2SO_4$ to give ca. 80% relative humidity [16]) as a carrier for gas for formic acid or hydrogen. The schematic diagram in Figure 1B shows the proposed reaction for formic acid vapor entering the salt cell, reacting at the palladium catalyst, formation of electrons (conducted into the electrode) and protons (conducted into the salt layer), and formation of CO_2 gas. The overall process is complex and factors influencing the reaction progress divers. In this report a first attempt is made to explore catalyst reactivity in the presence of salt electrolyte and to optimize conditions for gas phase reactions at salt | electrode | gas triple phase boundary contacts.

2. Experimental

2.1. Reagents

Palladium(II) chloride (99.9wt%), formic acid (95 wt%) and all ammonium salts (di-ammonium sulfate, ammonium nitrate, ammonium chloride, di-ammonium hydrogen phosphate, ammonium di-hydrogen phosphate) were obtained from Sigma-Aldrich (UK) and were used without further purification. Solutions were prepared with deionized water of resistivity 18.2 MΩ cm from a Thermo Scientific water purification system (Barnstead Nanopure). Nitrogen gas and hydrogen gas (Pureshield, BOC) were used.

2.2. Instrumentation

A three-electrode system was employed with a 3 mm diameter glassy carbon electrode (BAS), a Pt wire counter electrode, and a KCl-saturated calomel reference (SCE, Radiometer, Copenhagen) for Pd electrochemical deposition. A two-electrode electrochemical set-up was employed with a 3 mm diameter glassy carbon electrode (BAS) as the working electrode and a KCl-saturated calomel electrode (SCE, Radiometer, Copenhagen) as the counter-reference electrode in a custom-build salt electrolyte cell (see Figure 1 [7]). The SCE electrode is used here in the counter-reference mode only for low currents where the reference potential remains un-effected. A computer-controlled Autolab potentiostat (PGTAT 12, Ecochemie, NL) was used for data collection. All experiments were conducted at ambient temperature (293 ± 2 K). Transmission electron microscopy (TEM) images were obtained using a JEOL JEM1200EXII and scanning electron microscopy (SEM) images were obtained on a SEM6480LV system.

2.3. Procedure I.: Electro-Deposition of Pd Nanoparticle Catalysts Films

Pd nanoparticles on a glassy carbon electrode surface were deposited electrochemically [17] with an applied potential of -0.2 V vs. SCE from a 1 mM $PdCl_2$ solution in aqueous 0.1 M phosphate buffer (pH 2) with 0.1 M KCl. The potential was held for 90 s and then the electrode was removed, rinsed with deionized water, and dried in nitrogen flow. The resulting Pd nanoparticle film is relatively smooth (see SEMs in Figure 2A,B) and contains nanoparticles of ca. 6 to 12 nm diameter (see TEMs in Figure 2C,D). The film thickness can be estimated as 50 +/- 20 nm.

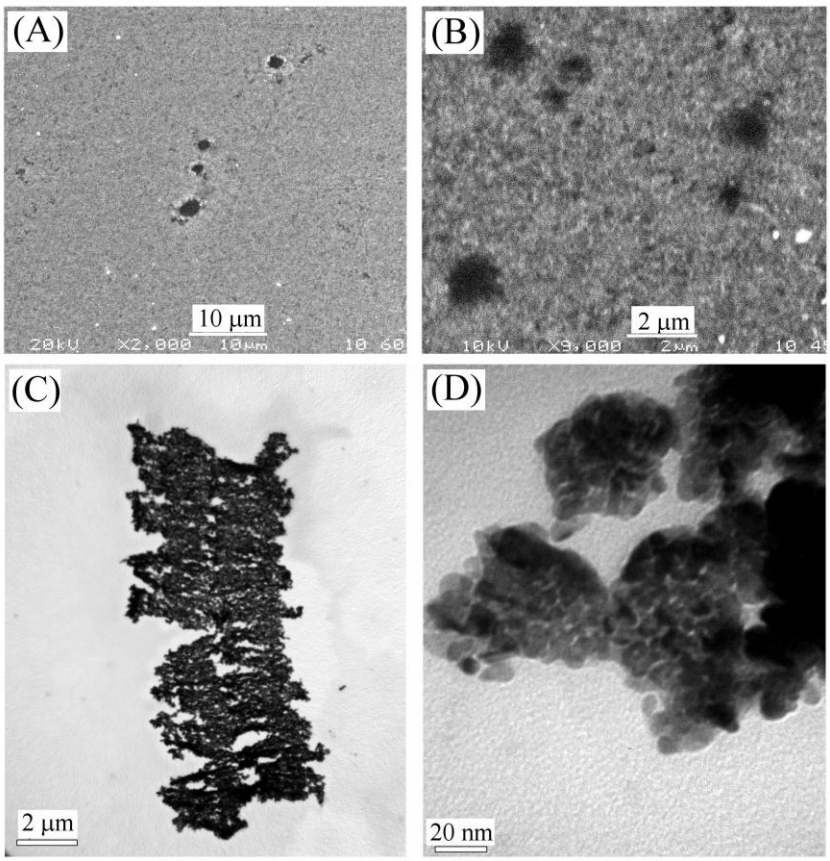

Figure 2. (A,B) SEM images of Pd nanoparticle films electro-deposited onto glassy carbon. Dark spots are likely to be caused by gas bubbles blocking the surface during deposition. (C,D) TEM images showing nano-Pd catalyst removed from the electrode surface and dispersed into ethanol with a pipette tip. (C) Pd catalyst film in low magnification and (D) Pd catalyst particles in high magnification.

2.4. Procedure II.: Salt | Gas | Electrode Contact and Gas Flow Cell Voltammetry

Mechanical grinding of ammonium salts was carried out using a pestle and mortar until a fine uniform grain was obtained. The salt was then placed into the chamber of the electrochemical cell with the counter-reference electrode in place. The working electrode was pushed into the cell to contact the salt. Nitrogen gas was passed first through a gas wash bottle containing saturated aqueous solution of $(NH_4)_2SO_4$ to give approximately 80% relative humidity [16]. For formic acid experiments the wash bottle was filled with pure (95%) or diluted formic acid instead. For hydrogen pulse experiments hydrogen gas was "bled" into the flow of nitrogen via a T-junction between wash bottle and cell (ca. 0.5 atm partial pressure).

3. Results and Discussion

3.1. Electrochemical Characterization of the Gas | $(NH_4)_2SO_4$ | Electrode Contact With and Without Nano-Palladium

A glassy carbon electrode is immersed into aqueous saturated $(NH_4)_2SO_4$ and investigated by cyclic voltammetry over a +1.0 to -1.0 V vs. SCE potential range. Without surface modification of the glassy carbon a clean background is observed without significant redox processes (see Figure 3). The palladium nanoparticle catalyst deposit is then applied in a chronoamperometric process (see experimental section) giving a porous film with particles of typically 6 nm to 12 nm diameter and approximately 50 nm average thickness (see Figure 2). With the Pd nanoparticle deposit immobilized on the glassy carbon electrode surface, and when immersed into aqueous saturated $(NH_4)_2SO_4$ (at pH 5.2), two prominent redox processes are observed (see Figure 3A). In the negative potential range at ca. -0.50 V vs. SCE a chemically reversible reduction is observed (process 1). This cathodic process is associated with the reduction of protons and subsequent adsorption of hydrogen into palladium metal [18,19]. The complexity of the reduction and back-oxidation peak signals and the peak-to-peak separation suggest the presence of surface intermediates. However, a general expression for redox process 1 can be tentatively assigned (see equation 1).

$$Pd(s) + 2\ H^+(aq) + 2\ e^-(m) \rightarrow Pd\text{-}H_2(s) \quad (1)$$

The effect of scan rate on the voltammetric signal is considerable and a switch in behaviour appears to occur from small peak-to-peak separation (at scan rates < 20 mVs^{-1}) to a wide peak-to-peak separation (at scan rates > 20 mVs^{-1}). A further voltammetric peak signal is observed in the positive

potential range at ca. 0.38 V vs. SCE (see process 2 in Figure 3A) consistent with the palladium nanoparticle surface oxidation and back-reduction [20] (see equation 2).

$$Pd(s) + H_2O(aq) \rightarrow PdO(s) + 2\,H^+(aq) + 2\,e^-(m) \quad (2)$$

The area under this oxidation peak (process 2) expressed as charge, ca. 125 μC, can be used to estimated the real area of the nano-palladium deposit (assuming ca. 500 μC cm^{-2}; this number has been obtained experimentally with a palladium wire in the same electrolyte solution) as 0.25 cm^2. This area is consistent with a film of 10 nm diameter palladium nanoparticles containing 0.8×10^{11} particles or a thickness of ca. 3 layers or about 30 nm (ignoring packing effects).

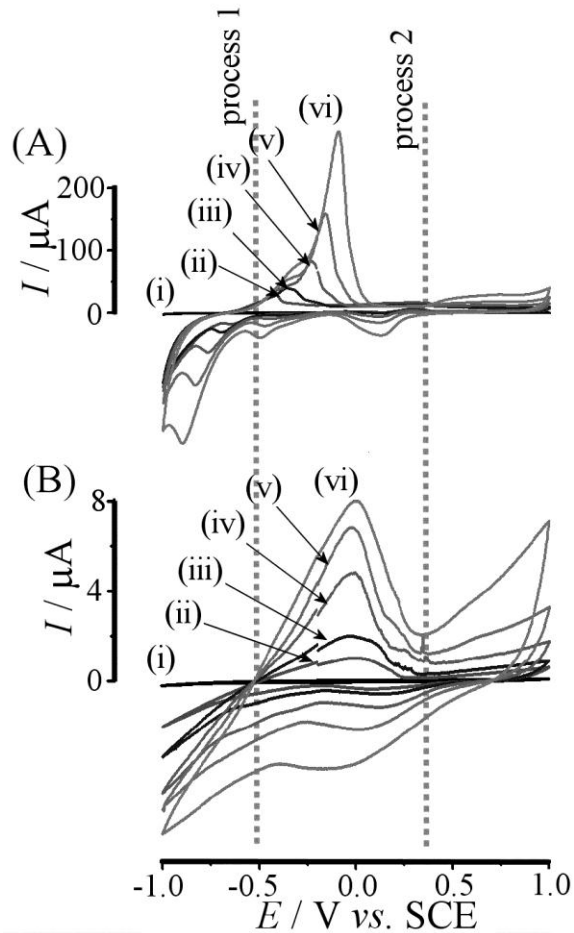

Figure 3. (A) Cyclic voltammograms (scan rate (i,ii) 10, (iii) 20, (iv) 50, (v) 100, and (vi) 200 mV s^{-1}) for a glassy carbon electrode (i) without and (ii-vi) with palladium nanoparticle deposit immersed in saturated aqueous $(NH_4)_2SO_4$ solution. (B) Cyclic voltammograms for the same

electrode in contact to $(NH_4)_2SO_4$ salt crystals with a flow of humidified (ca. 80% relative humidity) nitrogen.

When repeating these experiments in a salt matrix electrochemical cell [5] (see experimental), very similar voltammetric features are observed. Figure 3B shows data obtained as a function of scan rate. In the absence of Pd nanoparticles a featureless glassy carbon background is observed. With nano-palladium, processes 1 and 2 are observed in the presence of the salt matrix at potentials very similar to those observed in aqueous solution. Both processes are predicted to be sensitive to proton activity (see equations 1 and 2) and it can therefore be concluded that the proton activity in the electrochemically active zone at the electrode surface in contact to the salt is similar to that in aqueous saturated $(NH_4)_2SO_4$ solution. However, the magnitude of current responses with the salt contact is much lower compared to that for the aqueous electrode interface presumably due to the lower active contact area between electrode surface and salt (only point contacts).

The shape of the voltammetric response for the reduction and back-oxidation signal for process 1 at ca -0.5 V vs SCE is affected by uncompensated resistance (iR potential drop) as can be inferred from the linearly rising shape of the current response. Also for process 2 a shift in the peak position for the reduction of the oxidized palladium surface suggests a similar potential drop effect. In addition to these non-ideality or potential gradient effects, there is a possibility for pH gradients forming during processes in which protons are consumed or produced (see equations 1 and 2). Transport of ions into or away from the electrochemically active zone is limited and probably possible only via the surface of the salt crystals. The $(NH_4)_2SO_4$ crystals will provide some buffer effect to avoid highly alkaline conditions, but the formation of protons could result in considerable localized acidification (vide infra).

The approximate area under peaks (in terms of charge) for process 2 in Figure 3B is 10 μC suggesting (in comparison to the result in aqueous solution) a utilization of only approximately 20% of the palladium catalyst present at the glassy carbon electrode surface. Unknown in this approximation is the effect of the unusual reaction conditions on the formation of the surface oxide layer on palladium.

3.2. Electrochemical Oxidation of Formic Acid at $(NH_4)_2SO_4$ | Glassy Carbon Contacts with Nano-Palladium Catalyst

Next, a more complex process based on the electrocatalytic oxidation of formic acid at the nano-palladium catalyst is investigated. This process in aqueous media has been thoroughly studied [21,22]. Here the oxidation of formic acid vapor in the salt cell is investigated by flowing nitrogen through a wash bottle filled with 95% formic acid and then into the cell and past the Pd nanoparticle coated working electrode.

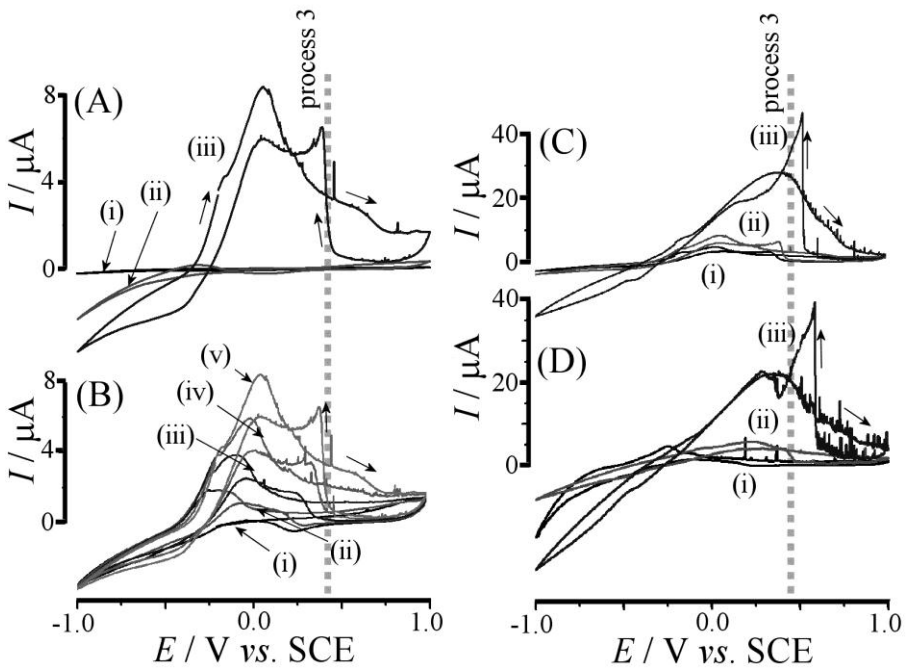

Figure 4. (A) Cyclic voltammograms (scan rate 10 mV s^{-1}, 5th cycle) for (i) a bare glassy carbon electrode in contact to $(NH_4)_2SO_4$ in humidified nitrogen, (ii) a Pd-coated glassy carbon electrode in contact to $(NH_4)_2SO_4$ in humidified nitrogen, and (iii) a Pd-coated electrode with formic acid saturated nitrogen (wash bottle with 95 % formic acid, nitrogen flow rate 90 cm^3 min^{-1}). (B) Consecutive potential cycles (i) to (v) for formic acid oxidation (95 % formic acid, Nitrogen flow

rate 90 cm^3 min^{-1}). (C) Cyclic voltammograms (scan rate 10 mV s-1, 5^{th} cycle) for formic acid oxidation (95 % formic acid, nitrogen flow rates (i) 30, (ii) 90, and (iii) 180 cm^3 min^{-1}). (D) Cyclic voltammograms (scan rate 10 mV s-1, 5^{th} cycle) for formic acid oxidation (85 % formic acid, nitrogen flow rates (i) 30, (ii) 90, and (iii) 180 cm^3 min^{-1}).

Figure 4A shows typical voltammetric responses. In the absence of palladium catalyst no significant current response is observed in the potential range investigated. Figure 4Aii shows the current responses for the palladium catalyst in contact to humidified nitrogen where processes 1 and 2 are observed. However, when nitrogen is passed through 95% formic acid, the formic acid vapor is interacting with the palladium catalyst and new redox processes are observed (Figure 4Aiii). Process 1 (hydrogen formation and oxidation) is observed with increased currents and shifted to approximately -0.3 V vs. SCE. When scanning the potential further positive a new oxidation is observed (see process 3) consistent with the oxidation of formic acid to carbon dioxide [23] (see equation 3).

$$Pd(s) + HCOOH(g) \rightarrow Pd(s) + CO_2(g) + 2\,H^+(salt) + 2\,e^-(m) \qquad (3)$$

There are several reaction steps required in this formic acid oxidation process and distinct pathways based on adsorbed formyl, formate, and CO intermediates have been suggested [24,25]. In the present study only the overall process is considered.

The oxidation currents for formic acid are most noticeable (i) during the forward scan directly after process 1 has occurred, and (ii) during the backward scan upon conversion of PdO at the nanoparticle surface back to “active” Pd metal catalyst. The anodic current spike is (see process 3) is typical for palladium catalysts [26] and indicative of both catalyst performance and pH conditions at the palladium catalyst surface. Data in Figure 4B show the current peaks increasing over consecutive potential cycles (possibly due to a slow spreading of the reaction zone). Figure 4C

shows cyclic voltammetry data obtained for three different gas flow rates. An increase in the nitrogen flow rate is causing an increase in the anodic current signal as well as in the shape of the voltammogram (note merging of process 1 and process 2 at higher flow rate). Figure 4D shows data for the flow rate dependence when the nitrogen is passed through 85% formic acid instead of 95% formic acid. At lower flow rates the formic acid oxidation process is substantially diminished, although at high flow rate the oxidation remains effective. Experiments with lower concentrations of formic acid suggest that the effectiveness of the formic acid evaporation rapidly diminishes with lower formic acid content in the liquid. This is at least in part due to non-ideality effects in this liquid mixture [27].

3.3. Electrochemical Oxidation of Formic Acid at the Salt | Palladium | Glassy Carbon Contact for Different Salts

The successful oxidation of formic acid vapor under $(NH_4)_2SO_4$ salt contact conditions suggests that conditions at the active palladium nanoparticle catalyst are similar to those anticipated for highly concentrated salt solutions. It is interesting to ask whether the choice of salt in this process can introduce beneficial or detrimental effects on the catalytic process. In a recent study the beneficial effects of ammonium cations on palladium catalysts have been reported [28]. Therefore, a range of ammonium salts was screened and dramatic effects on reactivity observed. Figure 5A shows data obtained in contact to ammonium nitrate. In humidified nitrogen (see Figure 5Ai) the familiar voltammogram with process 1 and process 2 is observed. With formic acid vapor in the nitrogen flow, however, the oxidation of formic acid to carbon dioxide is suppressed. An onset of this process (process 3) can be seen at ca. 0.9 V vs. SCE, but the characteristic catalytic oxidation does not occur. This effect is even more dramatic for NH_4Cl electrolyte (see Figure 5B). Nitrate and in particular chloride anions appear to strongly suppress the catalytic oxidation process at the

palladium surface. In the presence of chloride well-defined peak signals are seen where process 2 should occur. The charge under these oxidation peaks is approximately 150 μC (vide supra) suggesting substantial conversion of the palladium surface probably to $PdCl_2$ and loss of all catalytic activity.

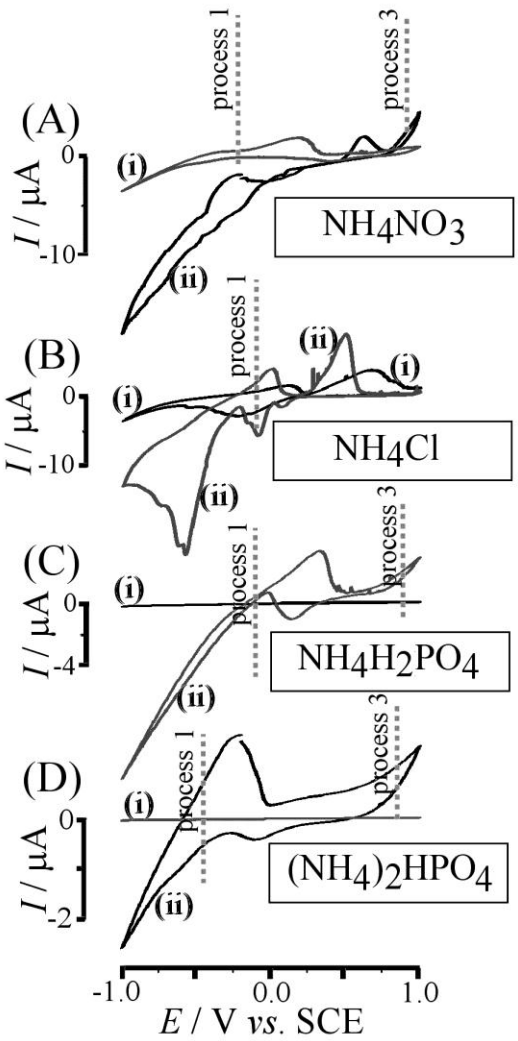

Figure 5. Cyclic voltammograms (scan rate 10 mVs^{-1}, 5^{th} cycle, nitrogen flow rate 30 cm^3 min^{-1}) for (i) humidified nitrogen and (ii) nitrogen saturated with 95% formic acid in contact to Pd nanoparticles and salt electrolyte: (A) NH_4NO_3, (B) NH_4Cl, (C) $NH_4H_2PO_4$, and (D) $(NH_4)_2HPO_4$.

The electrolyte salt $NH_4H_2PO_4$ was ineffective in the presence of humidified nitrogen, but did give

substantial current responses for formic acid vapor (see Figure 5C). The voltammetric response is dominated by the hydrogen process (process 1) at ca. -0.1 V vs. SCE but very little evidence for formic acid oxidation is observed. Similarly, for $(NH_4)_2HPO_4$ process 1 is dominating and formic acid oxidation appears ineffective. It is likely that in both cases the phosphate anion can block the palladium surface and suppress the catalytic process. A shift in the position of process 1 (see Figure 5C,D) can be explained with a change in the local pH in the reaction zone with the di-basic hydrogen phosphate introducing more alkalinity.

Perhaps surprisingly, ammonium sulphate emerges as a good choice for maintaining catalyst activity in high salt concentration environments. The list of salt systems studied is limited and exploratory. In future other better salt electrolyte systems are likely to help improving the palladium catalyst performance in the salt electrolysis cell.

3.4. Electrochemical Oxidation of Hydrogen at the Salt | Palladium | Glassy Carbon Contact

It is interesting to further explore process 1, the proton reduction / hydrogen oxidation reaction at the palladium catalyst immobilized at the glassy carbon electrode surface. The rapid detection of hydrogen gas is an important sensing problem [29,30] due to the challenge of achieving a rapid response without delay due to diffusion of hydrogen through a liquid layer. Hydrogen gas reaching the palladium | $(NH_4)_2SO_4$ salt contact should result in an anodic current response similar to that seen as process 1.

Figure 6 shows typical cyclic voltammetry responses for the palladium | $(NH_4)_2SO_4$ system in a flow of humid nitrogen. In the second potential cycle hydrogen gas is added into the nitrogen gas flow and an instantaneous increase in the anodic current is observed. The current pulse at ca. 0.8 V vs.

SCE reaches a plateau at ca. 8 μA consistent with the current expect for process 1 when extrapolating the iR-limited slope for process 1 to more positive potentials. The increase in current with more positive potential is clearly observed also for the second and third hydrogen pulse (see Figure 6ii).

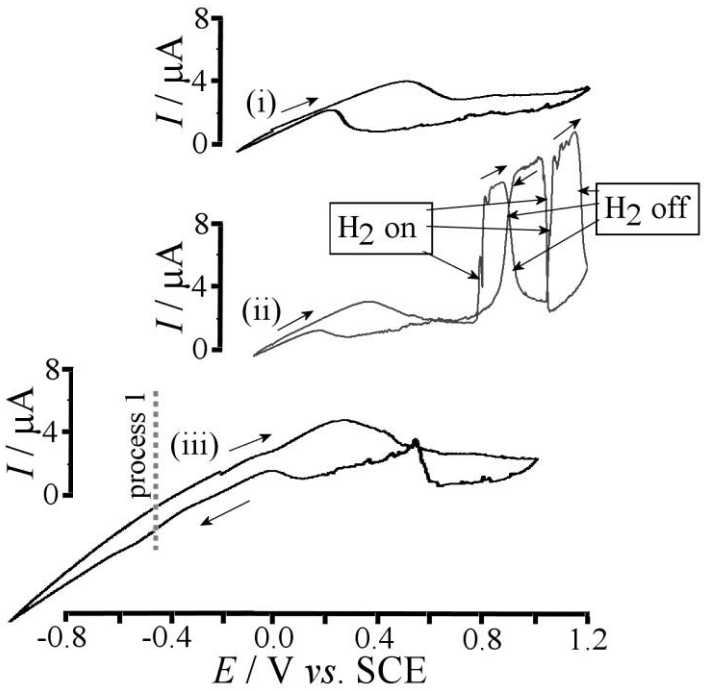

Figure 6. Cyclic voltammograms (scan rate 10 mVs^{-1}, gas flow rate 30 cm^3 min^{-1}, nitrogen gas with ca. 80% relative humidity) for a glassy carbon palladium | $(NH_4)_2SO_4$ interface: (i) first potential cycle, (ii) second potential cycle with three pulses of hydrogen added into the nitrogen flow, and (iii) third potential cycle again under humid nitrogen.

These preliminary data suggest that (i) the response time of the system is very fast and (ii) the current responses are limited by iR drop effects probably in the salt electrolyte. In future work the response time needs to be optimized (with improved cell design, better ion conductors, and better catalysts) and the linear range and sensitivity of the response to hydrogen gas needs to be further investigated.

4. Conclusions

Electrochemical processes at a glassy carbon – palladium nanoparticle – salt contact have been studied in the presence of humidified nitrogen and with two relevant redox systems: (i) the oxidation of formic acid and (ii) the oxidation of hydrogen. A dramatic effect of the type of salt on palladium catalyst reactivity has been established and ammonium sulphate is suggested as a suitable electrolyte salt. Redox processes at nano-catalyst – salt interfaces (or more generally catalyst – ion conductor interfaces) could be of wider use in particular when reactivity can be controlled or enhanced with choice of the appropriate salt (due to anion and cation surface effects, specific interactions, and pH effects). The magnitude of currents under two-electrode conditions with salt electrolytes is limited but in future devices based for example on MEAs or on generator-collector electrode pairs [31] could help developing salt electrode processes also for higher current applications.

Acknowledgements

This work was supported by CSC (China Scholarship Council, File No. 2010695033). We thank EPSRC for funding (DTC studentship for R.A.W. - EP/G03768X/1).

References

[1] F. Marken, A.M. Collins, J.D. Watkins, *PCCP*, 2011, **vol**, page.

[2] N.C. Cheng, R.A. Webster, M. Pan, S.C. Mu, L. Rassaei, S.C. Tsang, F. Marken, *Electrochim. Acta*, 2010, **55**, 6601.

[3] X.W. Yu, P.G. Pickup, *J. Power Sources*, 2008, **182**, 124.

[4] J.D. Morse, *Inter. J. Energy Res*., 2007, **31**, 576.

[5] S. Uhm, J.K. Lee, S.T. Chung, J. Lee, *J. Ind. Engineer. Chem.*, 2008, **14**, 493.

[6] D.T. Whipple, E.C. Finke, P.J.A. Kenis, *Electrochem. Solid State Lett*., 2010, **13**, D109.

[7] S.E.C. Dale, C.Y. Cummings, F. Marken, *Electrochem. Commun.*, 2011, **13**, 154.

[8] R. Parsons, T. VanderNoot, *J. Electroanal. Chem.*, 1988, **257**, 9.

[9] P. Waszczuk, T.M. Barnard, C. Rice, R.I. Masel, A. Wieckowski, *Electrochem. Commun.*, 2002, **4**, 599 and references cited therein.

[10] T.C. Johnson, D.J. Morris, M. Wills, *Chem. Soc. Rev.*, 2010, **39**, 81.

[11] F. Solymosi, A. Koos, N. Liliom, I. Ugrai, *J. Catal.*, 2011, **279**, 213.

[12] X.W. Yu, P.G. Pickup, *J. Power Sources*, 2008, **182**, 124.

[13] V. Mazumder, Y. Lee, S.H. Sun, *Adv. Func. Mater.*, 2010, **20**, 1224.

[14] E. Antolini, *Energy Environ. Sci.*, 2009, **2**, 915.

[15] X.W. Yu, P.G. Pickup, *J. Appl. Electrochem.*, 2011, **41**, 589.

[16] In: D.R. Lide, Editor, Handbook of Chemistry and Physics (74th ed.), CRC Press, London 1993, pp. 15–25.

[17] M.A. Ghanem, H. Hanson, R.G. Compton, B.A. Coles, F. Marken, *Talanta*, 2007, **72**, 66.

[18] V. Breger, E. Gileadi, *Electrochim. Acta*, 1971, **16**, 177.

[19] X.G. Zhang, T. Arikawa, Y. Murakami, K. Yahikozawa, Y. Takasu, *Electrochim. Acta*, 1995, **40**, 1889.

[20] L.D. Burke, J.K. Casey, *J. Electrochem. Soc.*, 1993, **140**, 1284.

[21] Electrocatalysis (Eds.: J. Lipkowski, P.N. Ross), Wiley-VCH, New York, 1998, p. 65.

[22] S.D. Han, J.H. Choi, S.Y. Noh, K. Park, S.K. Yoon, Y.W. Rhee, *Korean J. Chem. Engineer*.

2009, **26**, 1040.

[23] L. Meng, J. Jin, G.X. Yang, T.H. Lu, H. Zhang, C.X. Cai, *Anal. Chem*., 2009, **81**, 7271.

[24] M. Neurock, M. Janik, A. Wieckowski, *Faraday Disc*., 2008, **140**, 363.

[25] Y.X. Chen, M. Heinen, Z. Jusys, R.J. Behm, *Angew. Chem*., 2006, **45**, 981

[26] G. Samjeske, A. Miki, M. Osawa, J. Phys. Chem. C, 2007, **111**, 15074.

[27] A.K. Sum, S.I. Sandler, *Ind. Engineer. Chem. Res.*, 1999, **38**, 2849.

[28] H.Z. Li, Y.W. Tang, T.H. Lu, *Acta Physico-Chim. Sinica*, 2010, **26**, 3199.

[29] F. Yang, S.C. Kung, D.K. Taggart, R.M. Penner, *Sens. Lett.*, 2010, **8**, 534.

[30] F. Favier, E.C. Walter, M.P. Zach, T. Benter, R.M. Penner, *Science*, 2001, **293**, 2227.

[31] R.W. French, S.N. Gordeev, P.R. Raithby, F. Marken, *J. Electroanal. Chem.*, 2009, **632**, 206.